Processing and Application of Ceramics 19 [3] (2025) 293–300
https://doi.org/10.2298/PAC2503293Z

Modified calcium hexaaluminate with $La_2Ce_2O_7$ and corrosion resistance to cathode materials for lithium-ion batteries

Han Zhang[1,2], Guanyu Wang[1], Tianpeng Wen[1,*]

[1]*School of Metallurgy, Northeastern University, Shenyang, 110819, Liaoning, China*
[2]*Key Laboratory of Electromagnetic Processing of Materials, Ministry of Education, Northeastern University, Shenyang, 110819, Liaoning, China*

Received 18 June 2025; Received in revised form 27 August 2025; Accepted 20 September 2025

Abstract

In the present work calcium hexaaluminate (CA_6) was modified with different amounts of $La_2Ce_2O_7$ to improve sintering and explore its application possibility as the saggers for lithium-ion battery cathode material. It was found that the addition of $La_2Ce_2O_7$ causes incorporation of La^{3+} and Ce^{4+} ions into the CA_6 grains accompanied by the formation of cation vacancy defects. Such behaviour greatly supported the CA_6 grains to grow along the direction perpendicular to the basal plane and improved the densification of CA_6 materials. Typically, the bulk density of CA_6 with 6.0 wt.% $La_2Ce_2O_7$ addition exceeded 3.50 g/cm^3 and the apparent porosity decreased to below 3%. Moreover, the decrease in apparent porosity reduced the effective area between the Li^+ and CA_6 as well as inhibited the penetration of Li^+, leading to the improvement in the corrosion resistance and service life.

Keywords: *$CaAl_{12}O_{19}$, $La_2Ce_2O_7$, sintering, lithium-ion battery cathode materials, corrosion resistance*

I. Introduction

With the rapid development of the global economy and the extensive exploitation of non-renewable resources such as oil and coal, governments over the world are constantly seeking alternative new energy sources. Lithium-ion batteries have attracted widespread attention due to their advantages such as high specific energy, low self-discharge, fine cycling performance, no memory effect and green environmental protection, being currently considered to be the most promising high-efficiency secondary battery and the fastest developing chemical energy storage power source [1–4]. For lithium-ion batteries, the cathode is the main donor of lithium ions (Li^+) in battery systems, and therefore plays an important role in determining battery capacity, thermal stability and potential [5–8]. In other words, the development of cathode materials with advantages such as safety, economy, high performance and large capacity will effectively promote the widespread application of lithium-ion batteries.

At present, the mature cathode materials for application in lithium-ion batteries mainly include layered oxide materials such as Li_xMO_2 (M = Co, Mn, Ni), olivine type materials such as $LiFePO_4$ and spinel materials such as $LiMn_2O_4$ [9–14]. Solid phase sintering method is more favoured for the synthesis of cathode materials due to its simple process equipment and shorter production cycle. In the process of sintering cathode materials for lithium-ion batteries, it is necessary to select suitable saggers to improve the production efficiency of cathode materials, reduce the production costs and improve the production environment. Currently, oxide saggers such as cordierite, mullite and corundum are commonly used [15–17]. However, cordierite is easily corroded due to the strong alkalinity and corrosiveness of the lithium containing cathode materials, causing harmful impurities in the crucible and leading to a decrease in the quality of the cathode material. For the mullite, high silicon content and weak alkali resistance result in the peeling off of the material and mixing with the positive electrode material after long time use, affecting the purity of cathode materials. The alumina saggers are prone to cracking during the sintering process owing to the high thermal expansion coefficient of alumina, which declines its service life. Therefore, it is still a challenge to develop novel saggers to ensure the performance of lithium-ion battery cathode materials.

*Corresponding author: +86 24 83681576
e-mail: *wentianpeng@smm.neu.edu.cn*

Calcium hexaaluminate ($CaAl_{12}O_{19}$, CA_6) has been widely used in metallurgy, petrochemical and other fields due to its unique physical and chemical properties, including high melting point, excellent high temperature mechanical properties and chemical stability [18–23]. Recently, CA_6 exhibited the potential as the saggers for preparation of lithium-ion battery cathode materials based on its strong corrosion resistance under alkaline conditions [24,25]. However, the reaction between the components accompanied by volume expansion effect during the process of preparing CA_6 and its special platelet or plate-like particles inhibit the sinterability, densification process and mechanical properties [26–29]. Therefore, it is difficult for sintered CA_6 to reach full density even at high temperature and after multiple sintering. For this reason, the reaction sintered CA_6 material tends to have high porosity and may easily be corroded by the cathode materials of the lithium-ion battery, greatly reducing its service life and the purity of cathode materials. Consequently, high demands are urgently required for the dense and quality CA_6 materials used as the saggers for preparing the lithium-ion battery cathode materials.

Nowadays, numerous studies have looked at doping with small amount of metal cations to modify the structure of CA_6 and improve the comprehensive properties [22,23,30–36]. It has been found that the doped metal cations can substitute Ca^{2+} or Al^{3+} to form more defects in the structure of CA_6, promoting sintering and increasing the comprehensive properties. Although several studies have been done with metal cations as dopants in CA_6, the effect of composite additives and the coupling effect of two metal cations on its properties have not been explored. More importantly, there is little research on the modification of CA_6 as saggers for smelting the lithium-ion battery cathode materials, especially regarding the interfacial reaction and element migration behaviour between CA_6 saggers and lithium-ion battery cathode materials. Therefore, in the present work for the first time the effect of $La_2Ce_2O_7$ addition on structure evolution of CA_6 during sintering has been investigated. Subsequently, this work focused on the interfacial reaction characteristics between the CA_6 saggers and $LiMn_2O_4$ cathode materials, aiming to clarify the corrosion behaviour and mechanism of $LiMn_2O_4$ cathode materials in contact with CA_6 materials. This work will contribute to the application of CA_6 used as the saggers for smelting the lithium-ion batteries cathode materials and improve the corrosion resistance and service life of the saggers.

II. Experimental

2.1. Synthesis of $La_2Ce_2O_7$ particles

La_2O_3 (purity ≥99.99%, Sinopharm Chemical Reagent Co. Ltd.), and CeO_2 (purity ≥99.95%, Sinopharm Chemical Reagent Co. Ltd.) were used as raw materials to synthesize the $La_2Ce_2O_7$ particles by high temperature method. The La_2O_3 and CeO_2 mixture with the molar ratio of 1:1 was ball milled in ethanol for 6 h and then the obtained slurry was dried at 90 °C. Subsequently, the obtained La_2O_3 and CeO_2 mixture was uniaxially pressed into pellets with the diameter of 20 mm and the thickness of 20 mm under a pressure of 200 MPa, then the pellets were sintered at the peak temperature of 1600 °C for 5 h in air with the heating rate of 5 °C/min. Finally, the sintered pellets were crushed and ball milled for 2 h to obtain the $La_2Ce_2O_7$ powder.

2.2. Preparation of CA_6 materials

The Al_2O_3 (purity ≥99.0%, Sinopharm Chemical Reagent Co. Ltd.), $CaCO_3$ (purity ≥99.0%, Sinopharm Chemical Reagent Co. Ltd.) and the synthesized $La_2Ce_2O_7$ powders were employed as starting materials. The Al_2O_3 and $CaCO_3$ mixture (molar ratio of 6:1) was ball milled in ethanol for 4 h and then obtained slurry was dried at 90 °C. Subsequently, the obtained powders were pressed uniaxially into pellets with diameter of 30 mm and thickness of 30 mm under a pressure of 300 MPa and heat treated at 1200 °C for 1 h. The obtained samples were crushed to obtain the pre-synthesized raw materials with the powder size less than 75 μm. Furthermore, $La_2Ce_2O_7$ powder was introduced into the pre-synthesized raw materials with varying contents of 0, 2.0, 4.0 and 6.0 wt.%, corresponding to the samples denoted as CA-0, CA-2, CA-4 and CA-6, respectively. The mixed powders were repressed uniaxially into pellets with diameter of 20 mm and thickness of 20 mm at 100 MPa. Finally, the pellets were sintered at the peak temperature of 1600 °C for 2 h in air with the heating rate of 5 °C/min and then the samples were naturally cooled inside the furnace to room temperature.

2.3. Interfacial reaction between $LiMn_2O_4$ and CA_6

Li_2CO_3 (purity ≥98.0%, Sinopharm Chemical Reagent Co. Ltd.) and MnO_2 (purity ≥91.0%, Sinopharm Chemical Reagent Co. Ltd.) were employed as the precursors for preparation of the $LiMn_2O_4$ cathode materials. Static crucible method was selected to investigate the interfacial reaction between $LiMn_2O_4$ and CA_6 materials. The Li_2CO_3 and MnO_2 precursors with the molar ratio of 1:4 were placed on the surface of CA_6 pellet and then sintered at the peak temperature of 800 °C for 10 h in air with the heating rate of 5 °C/min. To analyse the corrosion behaviour the obtained sample was 10 times heated at 800 °C with dwell of 10 h.

2.4. Characterization

The densification parameters in terms of bulk density and apparent porosity of the sintered samples were measured via the Archimedes principle based on water as the medium. The phase compositions of the sintered and corroded samples were detected using X-ray diffraction (XRD, Model D500, Siemens, Germany) using Cu Kα radiation. The microstructure was examined by using

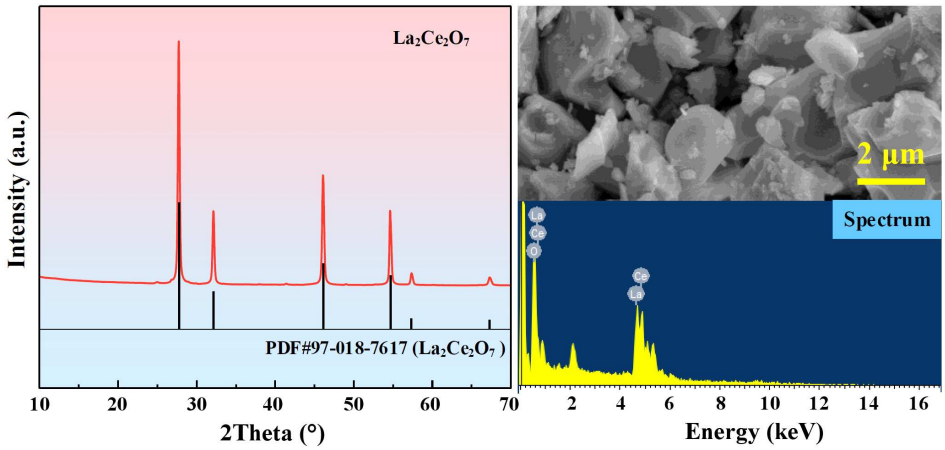

Figure 1. Phase composition and microstructure analysis of the synthesized $La_2Ce_2O_7$ powder

field emission scanning electron microscopy (FE-SEM, Model Ultra Plus, ZEISS, Germany) and transmission electron microscope (TEM, JEM-F200(HRP), Japan), and the elemental distribution was analysed by using the energy dispersive spectroscopy (EDS, Oxford, UK).

III. Results and discussion

3.1. Phase composition

Figure 1 shows the phase composition and microstructure analysis of the synthesized $La_2Ce_2O_7$ powder. According to the XRD phase identification results, single $La_2Ce_2O_7$ phase was observed with no observable impurity phase. Combining with the SEM image and EDS analysis, it was determined that the pure $La_2Ce_2O_7$ was successfully synthesized and can be used as the additive for CA_6 materials.

Figure 2 presents XRD patterns of the prepared CA_6 samples with various $La_2Ce_2O_7$ contents. As it can be seen, CA_6 was indexed as the main crystalline phase with a few observable XRD peaks of CA_2 ($CaAl_4O_7$) and Al_2O_3 phases in the sample CA-0 without $La_2Ce_2O_7$ addition. With the introduction of $La_2Ce_2O_7$, the Al_2O_3 phase further reacted with the CA_2 to form CA_6 phase. Meanwhile, the Al_2O_3 phase would also react with added $La_2Ce_2O_7$, forming $LaAl_{11}O_{18}$ and CeO_2 phases resulting in lack of detection of Al_2O_3 in the CA_6 samples with higher amount of $La_2Ce_2O_7$. In addition, a decrease in the diffraction peak of the CA_2 phase was also observed. Moreover, the CA_6 peaks exhibited a shift to lower 2θ values with increasing the $La_2Ce_2O_7$ addition from 0 to 6.0 wt.%, suggesting the uniform solid solution formation in the CA_6 samples with $La_2Ce_2O_7$ addition. Previous studies [23,23,30–36] have shown that the CA_6 lattices are good host structures to form solid solutions by replacing Al^{3+} with Fe^{3+}, Ti^{4+}, Zr^{4+}, etc. and Ca^{2+} with either alkaline-earth or rare-earth cations of similar radii. Based on the fact that cations Ca^{2+} (1.0 Å), Al^{3+} (0.53 Å), Ce^{4+} (0.97 Å) and La^{3+} (1.032 Å) have different radii, the in-

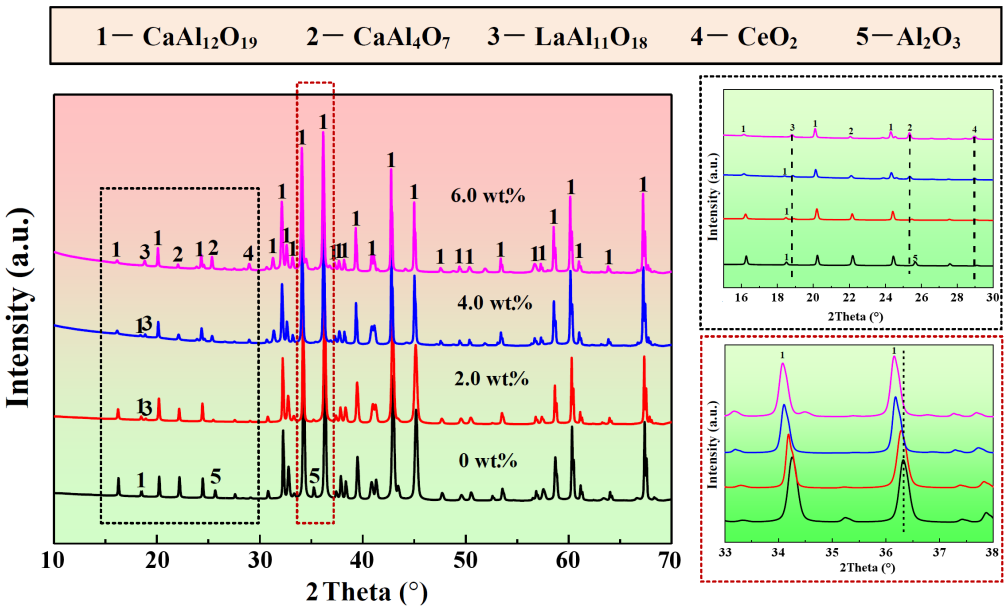

Figure 2. XRD spectra of the prepared CA_6 samples with various $La_2Ce_2O_7$ contents

troduced Ce^{4+} could substitute Al^{3+} in the spinel block of CA_6 lattice and the La^{3+} could substitute Ca^{2+} in the mirror layers of CA_6 lattice, along with the formation of $V^{\bullet}_{Al}$ and $V^{\bullet}_{Ca}$ vacancies according to Pauling's rule. Such behaviour was consistent with the previous research results [31,35,37]. The defect reactions in the CA_6 samples containing $La_2Ce_2O_7$ can be written as follows:

$$Ce^{4+} \xrightarrow{CA_6} Ce^{+}_{Al} + V^{\bullet}_{Al} \quad (1)$$

$$La^{3+} \xrightarrow{CA_6} La^{+}_{Ca} + V^{\bullet}_{Al} \quad (2)$$

Schematic diagram of ion migration in CA_6 lattice is presented in Fig. 3. It is worth noting that only part of Ce^{4+} is incorporated in the CA_6 lattice since CeO_2

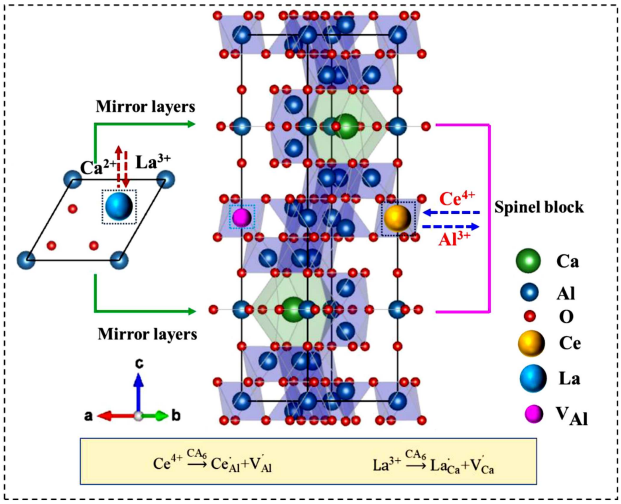

Figure 3. Schematic diagram of ion migration in CA_6 lattice

diffraction peaks were still detected in the XRD pattern of the CA-6 sample (Fig. 2), indicating that residual CeO_2 phase still existed in the CA_6 material.

3.2. Microstructure

Figure 4 displays SEM images of the sintered CA_6 samples with different $La_2Ce_2O_7$ addition. Generally, during formation CA_6 grains were exposed to high surface/interface energy anisotropy due to the low surface energy of the basal plane, driving a preferential grain growth along their basal plane (perpendicular to *c*-axes) [37]. Such behaviour continued until the elongated grains impinged upon each other. As a result, a typical platelet structure was observed in the CA_6 grains for the sample without $La_2Ce_2O_7$ addition, leading to the formation of the porous network. When $La_2Ce_2O_7$ was added to the CA_6 samples, the CA_6 grains transformed from platelet structure to hexagonal columnar equiaxed structure. This observation can be explained with the fact that the introduced $La_2Ce_2O_7$ could be dissolved into the CA_6 lattice to form uniform solid solution, namely, Ce^{4+} would substitute Al^{3+} in the spinel block of CA_6 lattice and the La^{3+} would substitute Ca^{2+} in the mirror layers of CA_6 lattice. The formation of the solid solution induced the structural modifications in the CA_6 lattice, thereby enhancing the O_2 diffusion rate along the *c*-axis, greatly supporting the CA_6 grains to grow along the direction perpendicular to the basal plane (*c*-axes). Furthermore, this positive effect was greatly promoted with the increase of $La_2Ce_2O_7$ content. For example, the CA_6 grains exhibited equiaxed morphologies with curved boundaries in the sample CA-6 with 6.0 wt.% of $La_2Ce_2O_7$, conducing to eliminate pores and form

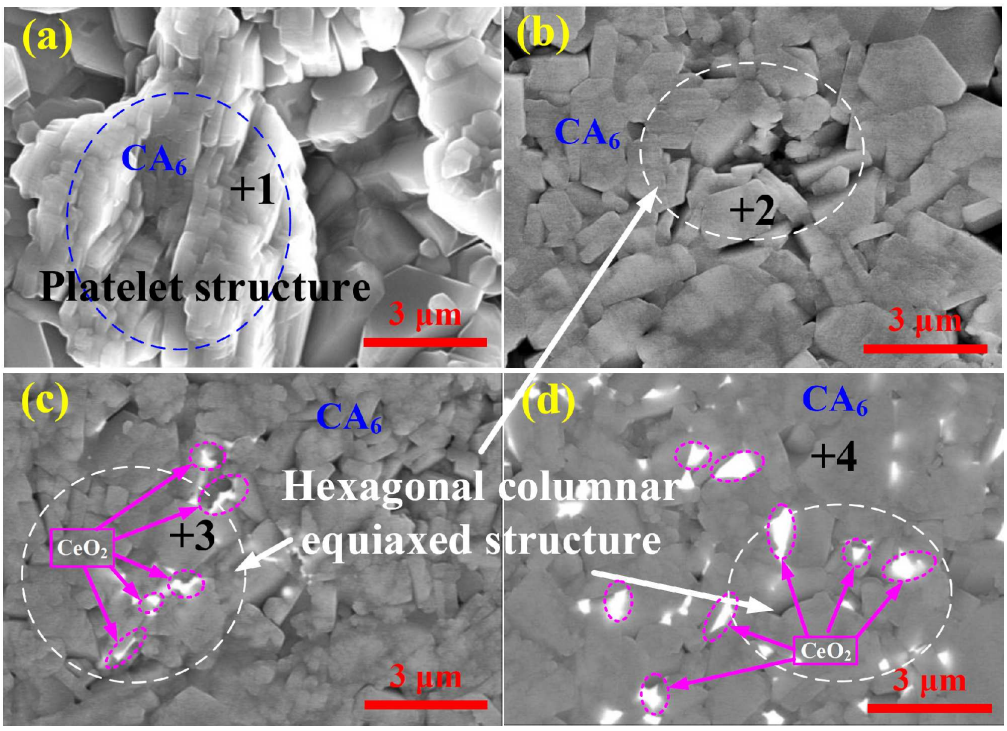

Figure 4. SEM images of the sintered samples: a) CA-0, b) CA-2, c) CA-4 and d) CA-6

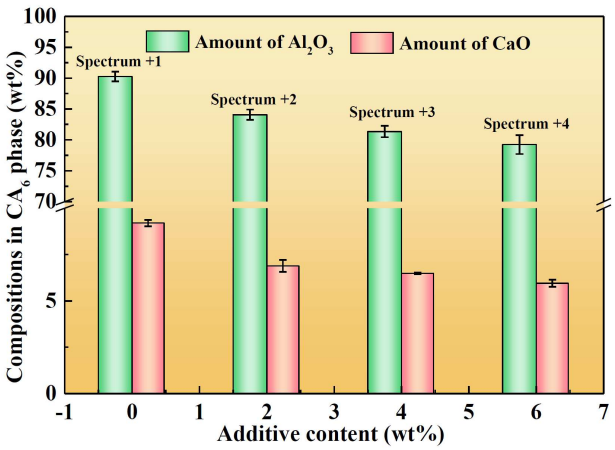

Figure 5. Variation of the amount of Al_2O_3 and CaO in CA_6 lattices as function of $La_2Ce_2O_7$ content

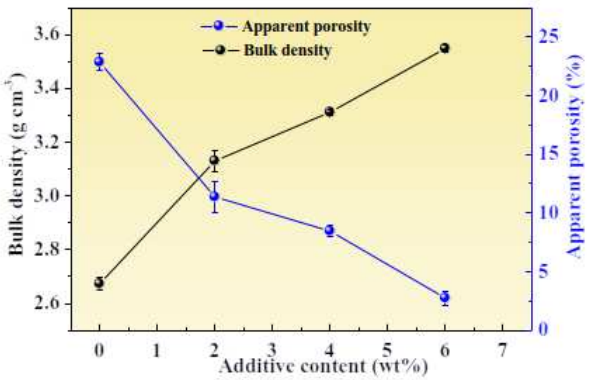

Figure 6. Variation in the apparent porosity and bulk density as function of $La_2Ce_2O_7$ content

highly dense structure. Moreover, CeO_2 will accumulate at the grain boundaries of CA_6 grains at high concentrations of additives, which would also contribute to the improvement in densification. To further verify the effect of $La_2Ce_2O_7$ on the CA_6 materials, the variation of the amounts of Al_2O_3 and CaO in the CA_6 lattices as function of $La_2Ce_2O_7$ content is given in Fig. 5. As it was expected, there is a significant decrease of Al_2O_3 and CaO amounts in the samples with $La_2Ce_2O_7$ addition, suggesting that La^{3+} and Ce^{4+} were dissolved into the CA_6 lattice.

Figure 6 presents the variation in the apparent porosity and bulk density of the sintered samples as function of $La_2Ce_2O_7$ addition. High apparent porosity exceeded 20% and corresponding low bulk density was observed for the sample CA-0 without $La_2Ce_2O_7$ addition, indicating the low sinterability due to slow diffusion rate of ions. When $La_2Ce_2O_7$ was introduced into the CA_6 samples, sintering process was greatly improved, with a trend of increasing relative density and decreasing apparent porosity. Typically, the bulk density reached 3.55 g/cm^3 while achieving an apparent porosity of only 2.75% when 6.0 wt.% $La_2Ce_2O_7$ was added to the CA_6 structure. Combined with the phase composition and microstructural evolution characteristics, the formation of the solid solution induced the structural modifications in the CA_6 lattice when the $La_2Ce_2O_7$ was introduced.

3.3. Interfacial reaction between $LiMn_2O_4$ and CA_6

Since the introduction of $La_2Ce_2O_7$ significantly improves the densification of CA_6, it was expected that this modified CA_6 material can be used as the saggers for preparing the lithium-ion battery cathode. Figure 7 displays XRD pattern, SEM and TEM images of the synthesized $LiMn_2O_4$ cathode material used as CA_6 saggers. The results indicate that the $LiMn_2O_4$ cathode materials were successfully prepared with Li_2CO_3 and MnO_2 as the raw materials at 800 °C through the following reaction:

$$2\,Li_2CO_3 + 8\,MnO_2 \longrightarrow 4\,LiMn_2O_4 + 2\,CO_2 + O_2 \quad (3)$$

To ensure the stability of the CA_6 saggers, the corrosion behaviour of CA_6 saggers during the smelting process of the $LiMn_2O_4$ cathode was investigated. XRD

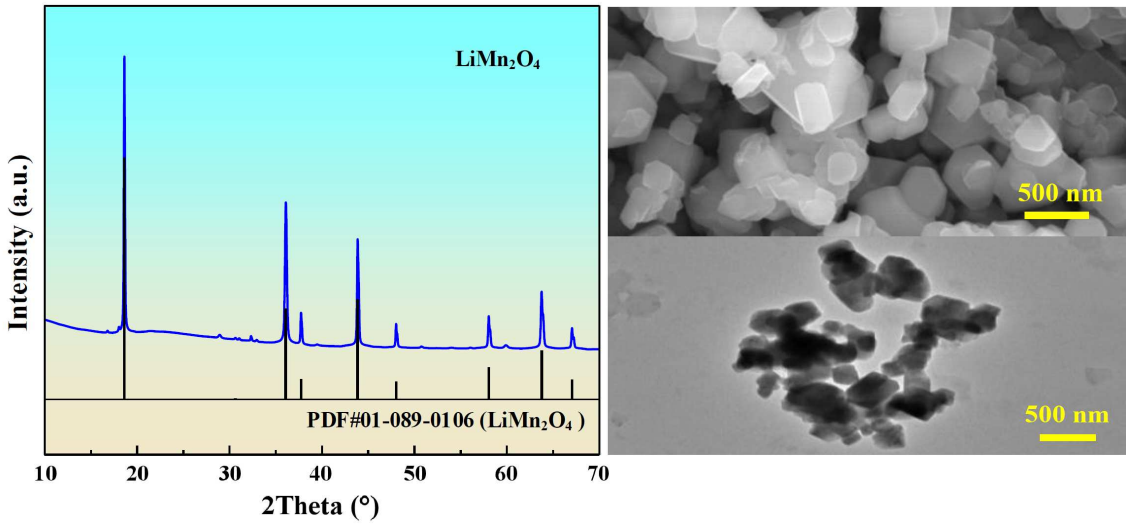

Figure 7. Phase composition and microstructure analysis of the synthesized $LiMn_2O_4$ cathode material

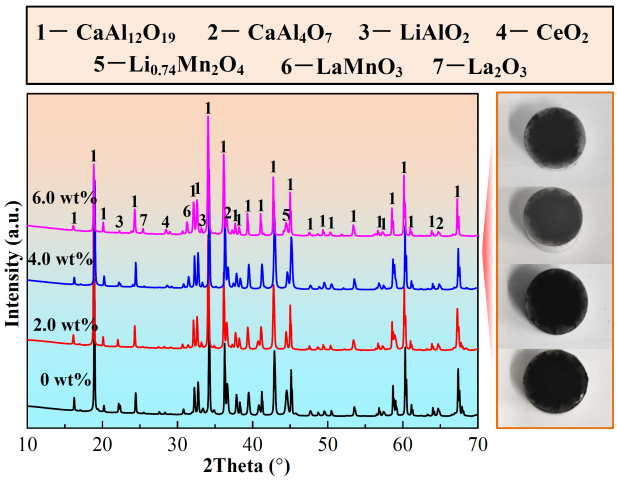

Figure 8. XRD spectra of the $CA_6/LiMn_2O_4$ samples after the corrosion test

spectra of the $CA_6/LiMn_2O_4$ samples after the corrosion test are depicted in Fig. 8. The analysis results reveal that $Li_{0.72}Mn_2O_4$, $LiAlO_2$ and $CaAl_4O_7$ phases are observed in the XRD patterns beside the CA_6 phase after the corrosion test. Simultaneously with the formation of $LiMn_2O_4$ according to reaction 3, Li^+ penetrates into the interior of the CA_6 material along the interface and reacted with CA_6 to form $LiAlO_2$ phase, accompanied by the formation of $CaAl_4O_7$. Moreover, the $LiMn_2O_4$ will be further oxidized to $Li_{0.74}Mn_2O_4$ in the air, accompanied by the formation of by-product Li_2O, which could also react with CA_6 to form $LiAlO_2$, causing structural changes in the materials and ultimately resulting in damage. The whole reaction process in the corrosion layer can be represented by the following reactions:

$$CaAl_{12}O_{19} + 4\,Li_2CO_3 \longrightarrow 8\,LiAlO_2 + CaAl_4O_7 + 4\,CO_2 \quad (4)$$

$$LiMn_2O_4 + 0.07O_2 \longrightarrow Li_{0.72}Mn_2O_4 + 0.14Li_2O_7 \quad (5)$$

$$CaAl_{12}O_{19} + 4\,Li_2O \longrightarrow 8\,LiAlO_2 + CaAl_4O_7 \quad (6)$$

After introducing $La_2Ce_2O_7$ to modify CA_6 materials, it was found that the diffraction peak intensities of $Li_{0.72}Mn_2O_4$, $LiAlO_2$ and $CaAl_4O_7$ phases in the XRD patterns were reduced, indicating that the reaction between Li^+ and CA_6 was inhibited. In other words, the corrosion resistance of the modified CA_6 was improved and more pronounced for the sample with higher $La_2Ce_2O_7$ content.

SEM-EDS analysis of the CA-0/$LiMn_2O_4$ and CA-6/$LiMn_2O_4$ samples after the corrosion test is illustrated in Fig. 9. As it can be seen, the corrosion layer composed of reaction layer and penetration layer was observed. For the CA_6 sample with 6.0 wt.% of $La_2Ce_2O_7$ (Fig. 9b), the thickness of corrosion layer (about 3.0 μm) is obviously thinner than that of the sample CA-0/$LiMn_2O_4$ without additives (about 20.0 μm). This observation was attributed to the decrease in apparent porosity of the modified CA_6 materials. On one hand, the decrease in apparent porosity reduced the effective area between the Li^+ and CA_6 materials [38], thereby reducing the reactivity between the $LiMn_2O_4$ cathode and the CA_6. On the other hand, the penetration of Li^+ into the interior of the CA_6 material was inhibited owing to the reduced Li^+ penetration channels caused by low apparent porosity. Meanwhile, the improvement of thermal shock resistance of the CA_6 ma-

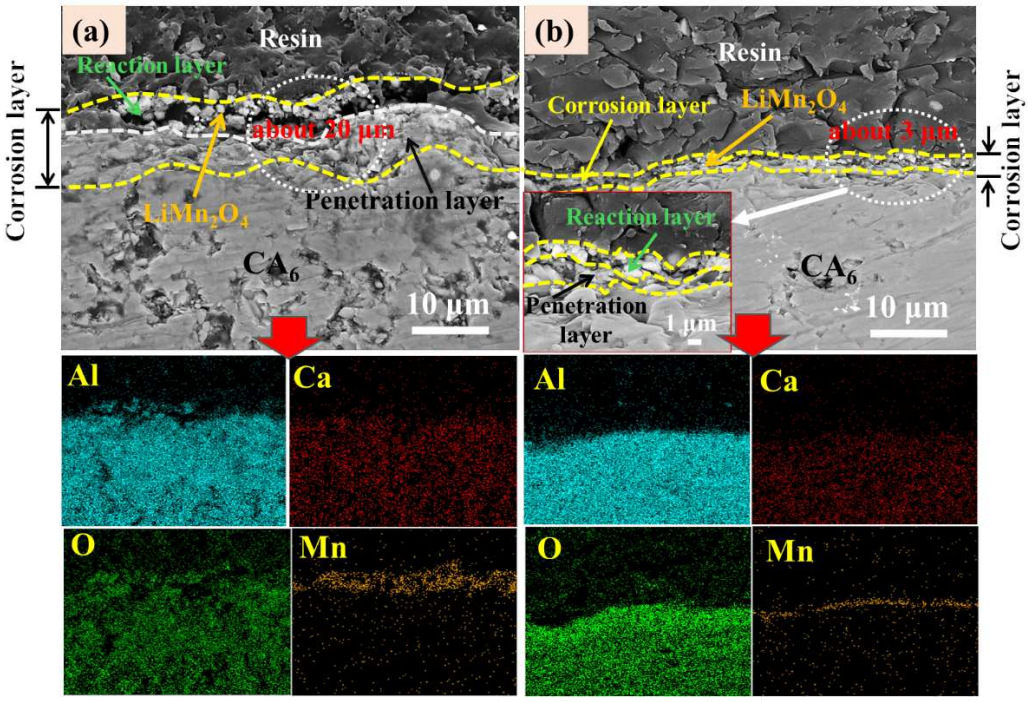

Figure 9. SEM-EDS analysis of the CA-0/$LiMn_2O_4$ and CA-6/$LiMn_2O_4$ samples after the corrosion test

terial reduced the dissolution of the CA_6 materials in the cathode material. The above behaviour would improve the corrosion resistance of the CA_6 material used as the saggers for preparing the lithium-ion battery cathode materials. In summary, low porosity and excellent thermal shock resistance gave the synergistic effect for improving the corrosion resistance of the CA_6 materials with $La_2Ce_2O_7$ additives.

IV. Conclusions

The present work investigated the effect of $La_2Ce_2O_7$ addition on structure evolution of CA_6 during sintering, aiming to achieve the modified CA_6 materials with improved densification. In addition, the interfacial reactions between the CA_6 saggers and $LiMn_2O_4$ cathode material were analysed to further clarify the corrosion behaviour $LiMn_2O_4$ cathode on the CA_6 materials. The results indicate that the La^{3+} and Ce^{4+} are incorporated into the CA_6 grains during sintering substituting Al^{3+} in the spinel block and Ca^{2+} in the mirror layers of the CA_6 lattice, respectively. These substitutions cause the formation of cation vacancies which greatly supported the CA_6 grains to grow along the direction perpendicular to the basal plane and improved the densification of CA_6 material. Typically, the relative density of CA_6 with 6.0 wt.% $La_2Ce_2O_7$ exceeded 90 %TD and the apparent porosity decreased to below 3%. Moreover, the decrease in apparent porosity reduced the effective area between the Li^+ and CA_6 as well as inhibited the penetration of Li^+, leading to the improvement in the corrosion resistance and service life and promoting its better application as the saggers for preparing the lithium-ion battery cathode.

Acknowledgement: This work was financially supported by the National Natural Science Foundation of China (No. 52204337), National Key Research and Development Program of China (2021YFB3701404), Liaoning Provincial Natural Science Foundation Joint Fund (General Support Program Project) (2023-MSBA-048) and the Fundamental Research Funds for the Central Universities (No. N2225035).

References

1. S. Kainat, J. Anwer, A. Hamid, N. Gull, S.M. Khan, "Electrolytes in lithium-ion batteries: advancements in the Era of Twenties (2020's)", *Mater. Chem. Phys.*, **313** (2024) 128796.
2. M.H. Shi, Y.H. Ren, J.Y. Cao, Z.Y. Kuang, X.J. Zhuo, H. Xie, "Current situation and development prospects of discharge pretreatment during recycling of lithium-ion batteries: A review", *Batteries Supercaps*, **7** (2024) e202300477.
3. D.Y. Chen, Q. Zhao, Y. Zheng, Y.Z. Xu, Y.H. Chen, J.H. Ni, Y. Zhao, "Recent progress in lithium-ion battery safety monitoring based on fiber bragg grating sensors", *Sensors*, **23** (2023) 5609.
4. J.H. Lim, D. Koh, S. Kolluri, M. Uppaluri, A. Subramaniam, V.R. Subramanian, "Efficient electrochemical state of health model for lithium-ion batteries under storage conditions", *J. Phys. Chem. C*, **127** (2023) 2183–2193.
5. P.K. Alaboina, M.J. Uddin, S.J. Cho, "Nanoprocess and nanoscale surface functionalization on cathode materials for advanced lithium-ion batteries", *Nanoscale*, **9** [41] (2017) 15736–15752.
6. P.Y. Guan, L. Zhou, Z.L. Yu, Y.D. Sun, Y.J. Liu, F.X. Wu, Y.F. Jiang, D.W. Chu, "Recent progress of surface coating on cathode materials for high-performance lithium ion batteries", *J. Energy Chem.*, **43** (2020) 220–235.
7. M.S. Islam, C.A.J. Fisher, "Lithium and sodium battery cathode materials: Computational insights into voltage, diffusion and nanostructural properties", *Chem. Soc. Rev.*, **43** [1] (2014) 185–204.
8. P.C. Zhu, D. Gastol, J. Marshall, R. Sommerville, V. Goodship, E. Kendrick, "A review of current collectors for lithium-ion batteries", *J. Power Sources*, **485** (2021) 229321.
9. X.X. Liu, Y.C. Tan, W.Y. Wang, C.H. Li, Z.W. Seh, L. Wang, Y.M. Sun, "Conformal prelithiation nanoshell on $LiCoO_2$ enabling high-energy lithium-ion batteries", *Nano Lett.*, **20** [6] (2020) 4558–4565.
10. X.Q. Ji, Q. Xia, Y.X. Xu, H.L. Feng, P.F. Wang, Q.Q. Tan, "A review on progress of lithium-rich manganese-based cathodes for lithium ion batteries", *J. Power Sources*, **487** (2021) 229362.
11. J. Zhu, G.L. Cao, Y.J Li, X.M. Xi, Z.M. Jin, B. Xu, W. Li, "Efficient utilisation of rod-like nickel oxalate in lithium-ion batteries: A case of NiO for the anode and $LiNiO_2$ for the cathode", *Scr. Mater.*, **178** (2020) 51–56.
12. C.L. Qin, Y.W. Li, S.X. Lv, J.Y. Xiang, C.L. Wang, X.G. Zhang, S. Qiu, G. Yushin, "Enhancing electrochemical performance of $LiFePO_4$ by vacuum-infiltration into expanded graphite for aqueous Li-ion capacitors", *Electrochim. Acta*, **253** (2017) 413–421.
13. X.B. Zhu, T.G. Lin, E. Manning, Y.C. Zhang, M.M. Yu, B. Zuo, L.Z. Wang, "Recent advances on Fe- and Mn-based cathode materials for lithium and sodium ion batteries", *J. Nanopart. Res.*, **20** (2018) 160.
14. R.Z. Yu, X.H. Zhang, T. Liu, L. Yang, L. Liu, Y. Wang, X.Y. Wang, H.B. Shu, X.K. Yang, "Spinel/layered heterostructured lithium-rich oxide nanowires as cathode material for high-energy lithium-ion batteries", *ACS Appl. Mater. Interfaces*, **9** (2017) 41210–41223.
15. P.T. Zhai, L.G. Chen, Y.M. Yin, S.P. Li, D.F. Ding, G.T. Ye, "Interactions between mullite saggar refractories and Li-ion battery cathode materials during calcination", *J. Eur. Ceram. Soc.*, **38** [4] (2018) 2145–2151.
16. K. Xiang, S.J. Li, Y.B. Li, H.L. Wang, R.F. Xiang, "Interactions of Li_2O volatilized from ternary lithium-ion battery cathode materials with mullite saggar materials during calcination", *Ceram. Int.*, **48** [16] (2022) 23341–23347.
17. H.P.A. Alves, R.A. Junior, L.F.A. Campos, R.P.S. Dutra, J.P.F. Grilo, F.J.A. Loureiro, D.A. Macedo, "Structural study of mullite based ceramics derived from a mica-rich kaolin waste", *Ceram. Int.*, **43** [4] (2017) 3919–3922.
18. A. Altay, C.B. Carter, P. Rulis, W.-Y. Ching, I. Arslan, M.A. Gülgün, "Characterizing CA_2 and CA_6 using ELNES", *J. Solid State Chem.*, **183** [8] (2010) 1776–1784.
19. V.K. Singh, K.K. Sharma, "Low-temperature synthesis of calcium hexa-aluminate", *J. Am. Ceram. Soc.*, **85** [4] (2002) 769–772.
20. L.C. Xu, E.H. Wang, X.M. Hou, J.H. Chen, Z.J. He, T.X.

Liang, "Effect of incorporation of nitrogen on calcium hexaaluminate", *J. Eur. Ceram. Soc.*, **40** [15] (2020) 6155–6161.

21. C. Dominguez, J. Chevalier, R. Torrecillas, L. Gremillard, G. Fantozzi, "Thermomechanical properties and fracture mechanisms of calcium hexaluminate", *J. Eur. Ceram. Soc.*, **21** (2001) 907–917.
22. T.P. Wen, Y. Jin, J.K. Yu, Z.G. Yan, Z.Y. Liu, L. Yuan, "Effect of Nb_2O_5 additive on the sintering behavior and properties of calcium hexaluminate", *Constr. Build. Mater.*, **385** (2023) 131534.
23. T.P. Wen, Y. Jin, Z.G. Yan, Z.Y. Liu, J.K. Yu, L. Yuan, G. Yuan, "Optimization design of Ta_2O_5-doped calcium hexaaluminate with improved sintering densification and properties for metallurgical application", *J. Alloys Compd.*, **945** (2023) 169297.
24. H.L. Wang, Y.B. Li, X.H. He, B. Yin, R.F. Xiang, S.J. Li, S.Q. Li, "Anti-corrosion effect of insulating firebrick coated with CA_6 in the calcination of lithium-ion cathode materials", *Ceram. Int.*, **48** (2022) 36723–36730.
25. C.Q. Gan, H. Zhang, H.Z. Zhao, Y. Zhang, H.H. He, "Firing properties and erosion resistance of hibonite-cordierite sagger", *Ceram. Int.*, **48** [20] (2022) 30589–30597.
26. A.G. Ersson, E.M. Johansson, S.G. Järås, "Techniques for preparation of manganese-substituted lanthanum hexaaluminates", *Stud. Surf. Sci. Catal.*, **118** (1998) 601–608.
27. D. Asmi, I.M. Low, "Physical and mechanical characteristics of in-situ alumina/calcium hexaluminate composites", *J. Mater. Sci. Lett.*, **17** (1998) 1735–1738.
28. V.K. Singh, K.K. Sharma, "Low-temperature synthesis of calcium hexa-aluminate". *J. Am. Ceram. Soc.*, **85** [4] (2002) 769-772.
29. L. Xu, M. Chen, L.Y. Jin, X.L. Yin, N. Wang, L. Liu, "Effect of ZrO_2 addition on densification and mechanical properties of $MgAl_2O_4$-$CaAl_4O_7$-$CaAl_{12}O_{19}$ composite", *J. Am. Ceram. Soc.*, **98** (2015) 4117–4223.
30. J.H. Chen, H.Y. Chen, W.J. Mi, Z. Cao, B. Li, C.J. Liang, "Substitution of Ba for ca in the structure of $CaAl_{12}O_{19}$", *J. Am. Ceram. Soc.*, **100** [1] (2017) 413–418.
31. Z. Cormack, "Defects in $BaMgAl_{10}O_{17}$: Eu^{2+} blue phosphor", *J. Electroceram.*, **10** [3] (2003) 179–191.
32. P.M. Doyle, P.F. Schofield, A.J. Berry, A.M. Walker, K.S. Knight, "Substitution of Ti^{3+} and Ti^{4+} in hibonite ($CaAl_{12}O_{19}$)", *Am. Mineral.*, **99** [7] (2014) 1369–1382.
33. L. Liu, T. Onda, Z. Chen, "Microstructural evolution of Ti^{4+}-doped calcium hexaaluminate ceramics", *Ceram. Int.*, **46** (2020) 12897–12901.
34. J. Lu, Y.X. Pan, J.G. Wang, X.A. Chen, S.M. Huang, G.K. Liu, "Reduction of Mn^{4+} to Mn^{2+} in $CaAl_{12}O_{19}$ by co-doping charge compensators to obtain tunable photoluminescence", *RSC Adv.*, **3** [14] (2013) 4510–4513.
35. T.P. Wen, L. Yuan, E.D. Jin, T. Liu, C. Tian, J.K. Yu, "Effect of CeO_2 addition on the sintering behavior of the alumina-rich calcium aluminate ceramics", *Int. J. Appl. Ceram. Technol.*, **17** (2020) 1761–1768.
36. L. Xu, M. Chen, X.L. Yin, L. Liu, "Effect of TiO_2 addition on densification and mechanical properties of $MgAl_2O_4$-$CaAl_4O_7$-$CaAl_{12}O_{19}$ composite", *Ceram. Int.*, **42** [12] (2015) 9844–9850.
37. M.K. Cinibulk, "Hexaluminates as a cleavable fiber-matrix interphase: synthesis, texture development, and phase compatibility", *J. Eur. Ceram. Soc.*, **20** (2000) 569–582.
38. P. Ji, Z. Liu, G.C. Zhang, Z.J. Peng, J.K. Yu, L. Yuan, "Effects of $La_2Ce_2O_7$ on the phase composition, microstructure, wetting behaviour and corrosion resistance of magnesia refractory", *J. Alloys Compd.*, **1010** (2025) 177390.